Dalton Transactions

ROYAL SOCIETY OF CHEMISTRY

PAPER

View Article Online
View Journal | View Issue

Cite this: *Dalton Trans.*, 2025, **54**, 14716

Heterodinuclear Cu(I)/Mo(VI) chemistry with bifunctional dibenzobarrelene ligands

A. M. Buddhika Chandima, [a] Griffyn Sgro, [a] Sierra M. Hilditch, [d] Umesh I. Kaluarachchige Don,[a] Cassandra L. Ward,[b] Dennis P. Anderson,[b] Limor Herman,[c] Dmitri Gelman,*[c] Richard L. Lord *[d] and Stanislav Groysman *[a]

Bifunctional dibenzobarrelene ligands combining diphosphine with diol or other potentially bidentate functionalities are well-known mononucleating ligands for middle and late transition metals. These ligands generally exhibit tetradentate coordination, in which a metal is coordinated by [PC(sp^3)P] 3-dimensional pincer and an additional alkoxide donor. These ligands can also be envisioned as heterodinucleating ligands, which coordinate a soft, late metal (*via* the diphospine) and a hard, early metal (*via* the diolate); the heterodinucleating reactivity of these ligands has not been studied. Herein we describe our initial studies on Cu(I)/Mo(VI) chemistry of the diphosphine/diol ligand **L^{1}H$_2$**; it is compared with the dibenzobarrelene ligand combining diphosphine with diester (**L^2**). Both ligands led to stable Cu(I) complexes in which the ligand coordinates as a bidentate diphosphine. Spectroscopic characterization (carried out in CD_2Cl_2) revealed an AB system for the diastereotopic phosphine groups in ^{31}P {^{1}H} NMR spectrum. The phosphorus signals appear as an AB system due to the large values of $^2J_{P-P}$, 120–150 Hz. ^{63}Cu NMR spectroscopy (conducted in concentrated CD_3CN solutions) revealed broad Cu signals at, or below, room temperature. The observation of a quadrupolar ^{63}Cu (I = 3/2) signal was accompanied by the broadening of the ^{31}P signals, which now appear as a single broad peak. The reaction of both ligands with $(Et_4N)_2[MoO_4]$ failed to form well-defined products. Treatment of $[Cu(NCMe)_2(L^1H_2)](PF_6)$ with $(Et_4N)_2[MoO_4]$, followed by recrystallization from DMSO/ether, revealed the structure of a trinuclear complex $[MoO_2(\mu_2\text{-}O)_2\{Cu(DMSO)(L^1H_2)\}_2]$ in which one Mo(VI) center is linked with two Cu(I) centers *via* oxo bridging ligands. In DMSO solution, the trinuclear complex likely forms discrete ionic species $[Cu(DMSO)_2(L^1H_2)]_2[MoO_4]$ or $[Cu(DMSO)_2(L^1H_2)][Et_4N][MoO_4]$.

Received 6th June 2025,
Accepted 9th September 2025

DOI: 10.1039/d5dt01337b

rsc.li/dalton

Introduction

There is significant interest in the development of new heterodinucleating ligands, in the context of cooperative bimetallic activation of small molecules and synergistic catalysis.[1–5] Heterodinucleating ligands can provide structural support for heterobimetallic complexes, control metal–metal distances, and determine the orientation of the substrate. Heterodinucleating ligands can be particularly useful in supporting models of metalloenzyme active sites in the absence of a protective protein environment.

Mo–Cu carbon monoxide dehydrogenase (CODH) is an aerobic enzyme featuring a heterobimetallic [Mo^{VI}O$_2$–S–Cu^{I}] active site that efficiently catalyzes oxidation of toxic CO to relatively benign CO_2.[6,7] A variety of unsupported structural models of Mo–Cu CODH have been reported,[8] where [Mo(VI)–(μ_2-S)$_n$–Cu(I)] (n = 1, 2) was assembled with the aid of one[9–11] or two sulfido (or mixed sulfido/oxo) bridges.[12–14] However, these models have not demonstrated coordination and activation of CO, or a CO-like substrate like isocyanide, due to (i) coordinative oversaturation at Cu(I) and (ii) insufficient stability. An alternative approach towards the design of a more stable Mo–Cu CODH functional model potentially featuring coordinatively unsaturated Cu(I) involves heterodinucleating ligands that are not direct structural mimics of the enzyme active site. We investigated a series of xanthene-based heterodinucleating ligands that combine a catecholate donor for Mo(VI) with iminopyridine/aminopyridine for Cu(I) or related soft metals.[15–18] These ligands exhibited formation of Mo(VI)–Cu(I) complexes in the absence of a direct single-atom (sulfido/oxo) bridge; we have also described a Mo(VI)–Mo(0) complex in

[a]*Department of Chemistry, Wayne State University, 5101 Cass Ave., Detroit, MI 48202, USA. E-mail: groysman@wayne.edu*
[b]*Lumigen Instrument Center, Wayne State University, 5101 Cass Avenue, Detroit, Michigan 48202, USA*
[c]*Institute of Chemistry, The Hebrew University, Edmond Safra Campus, Givat Ram, 91904 Jerusalem, Israel. E-mail: dmitri.gelman@mail.huji.ac.il*
[d]*Department of Chemistry, Grand Valley State University, 1 Campus Drive, Allendale, Michigan 49401, USA. E-mail: lordri@gvsu.edu*

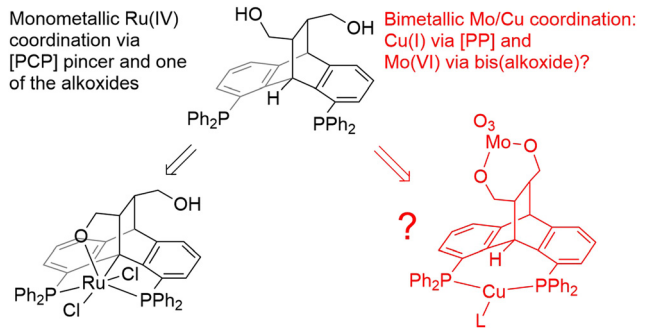

Fig. 1 Previously observed mononucleating and proposed dinucleating coordination mode of dibenzobarrelene ligand L^1H_2.

which the metals were bridged by a single oxo and Mo(0) coordinated CO ligands. Some of the models described above also enabled cooperative bimetallic reactivity, albeit not with the desired substrates (CO or CNR).[15] Given the promising reactivity enabled by this approach, we decided to probe additional heterodinucleating ligands towards this problem.

The dibenzobarrelene scaffold (Fig. 1) provides an underexplored framework for the construction of heterodinucleating ligands. A variety of [PC(sp^3)P] 3-dimensional pincer ligands for middle and late transition metals and their reactivity have been described by the Gelman group (for selected references, see below). These ligands are conveniently synthesized by cycloaddition of 1,8-bis-(diphenylphosphino)anthracene with various alkenes. Recently reported examples of dibenzobarrelene-ligated PCP complexes include high-oxidation-state Ni and Ru hydrosilylation catalysts,[19,20] and Ir/Pd-based CO_2 hydrogenation catalysts.[21–24] Most of these ligands employ additional donors appended to the alkene functionality, such as alkoxide, carboxylate, or ether. While these donors are generally capable of coordination to the [PCP]-bound metal (exemplified by the Ru(IV) complex in Fig. 1, left),[20] they can also be envisioned to chelate another metal, particularly if the diphosphine coordination site does not involve binding through the central carbon (Fig. 1, right).[25] Herein we report our initial results on the Mo(VI)/Cu(I) coordination chemistry and reactivity of selected ligands in the context of Mo–Cu CODH. We demonstrate that while L^1 does not coordinate the metals in the expected fashion, it nevertheless is capable of forming a rare discrete {Mo(VI)–O–Cu(I)–O–Mo(VI)} heterotrinuclear species.[26–30] Given the structural proximity of Mo(VI)–oxo and Cu(I), and the semi-labile position at Cu(I) (occupied by the solvent molecule), this heterotrinuclear species could serve as a viable candidate for the reactivity studies in the future.

Results and discussion

Ligands synthesis

Two ligands were investigated in this work, $\mathbf{L^1H_2}$ and $\mathbf{L^2}$ (Scheme 1). $\mathbf{L^1H_2}$ combines diphosphine and diol potential chelates. Synthesis, characterization, and reactivity of $\mathbf{L^1H_2}$ (as mononucleating tetradentate ligand for middle and late transition metals) has been previously reported by the Gelman group.[31] $\mathbf{L^2}$ replaces the alcohols with aprotic methyl ester functional groups. Whereas $\mathbf{L^1H_2}$ can potentially serve as a dinucleating ligand, coordinating Cu(I) *via* the diphosphine chelate, and Mo(VI) by the diol(ate), $\mathbf{L^2}$ is expected to coordinate Cu(I) only. $\mathbf{L^2}$ has not been previously reported; its synthesis and characterization are closely related to previously reported dibenzobarrelene ligands and provided in the Experimental section.[32]

Synthesis and characterization of Cu(I) complexes with L^1H_2 and L^2

Treatment of an acetonitrile solution of $[Cu(NCMe)_4](PF_6)$ (NCMe for acetonitrile) with a dichloromethane solution of $\mathbf{L^1H_2}$ produced a pale yellow solution. Subsequent work-up yielded $[Cu(NCMe)_2(L^1H_2)](PF_6)$ (**1**-NCMe) as a white solid. The complex was characterized by ^{1}H, ^{13}C{^{1}H}, and ^{31}P {^{1}H} NMR spectroscopy, and high-resolution mass spectrometry (HRMS). HRMS confirms the formation of the Cu(I) complex with $\mathbf{L^1H_2}$, demonstrating the molecular ion at m/z = 697.1434 (calculated m/z = 697.1486 for $[Cu(L^1H_2)]^+$). ^{1}H NMR demonstrates significant changes in the $\mathbf{L^1H_2}$ spectrum as a result of Cu(I) complexation. Both bridgehead protons are present, consistent with the bidentate coordination of the ligand. However, while one of the bridgehead protons is virtually unaffected (4.28 ppm in **1**-NCMe *vs.* 4.32 ppm in $\mathbf{L^1H_2}$, CD_2Cl_2), the other shifts upfield by 1 ppm (4.98 ppm in **1**-NCMe *vs.* 5.95 ppm in $\mathbf{L^1H_2}$), possibly due to anagostic interactions with the nearby Cu(I).[33] The ^{1}H NMR spectrum suggests the ligation of two molecules of CH_3CN in solution to Cu(I). A ROESY experiment (CD_3CN) suggested *trans* disposition of the methine hydrogens (α to the CH_2OH groups), which is consistent with X-ray structure of $[Cu(DMSO\text{-}d_6)_2(L^1H_2)](PF_6)$ (**1**-DMSO, DMSO is dimethyl sulfoxide, see below) suggesting "chelating" nature of the diol functionality. ^{13}C {^{1}H} NMR contains several doublet resonances due to the $^1J_{C-P}$ and $^2J_{C-P}$ coupling. The spectrum also contains a prominent triplet resonance at 42.33 ppm ($^4J_{C-P}$ = 15 Hz), likely due to the long-range coupling of the bridgehead carbon to both P atoms.[34] The HSQC spectrum demonstrates correlation of this peak to the ^{1}H NMR signal at 4.98 ppm, supporting its assignment as the bridgehead carbon facing Cu(I).

Another notable difference between the ligand and **1**-NCMe is observed in ^{31}P {^{1}H} NMR spectrum. Significantly, $\mathbf{L^1H_2}$ (and $\mathbf{L^2}$ as well) is asymmetric and therefore it displays two chemically inequivalent phosphorus nuclei. The spectrum of the ligand gives rise to an AX pattern featuring two doublets with the relatively small J_{P-P} = 13 Hz (Fig. 2, bottom). The coupling results from the through-space ^{31}P–^{31}P interaction, due to phosphorus anisochronous nuclei and the rigidity of the dibenzobarrelene backbone.[35–37] In contrast, **1**-NCMe exhibits an AB system, with relatively small $\Delta\upsilon$ = 241 Hz and large J_{P-P} = 119 Hz (Fig. 2, middle). Such a high value of J_{P-P} suggests $^2J_{P-P}$ coupling through Cu(I), which coordi-

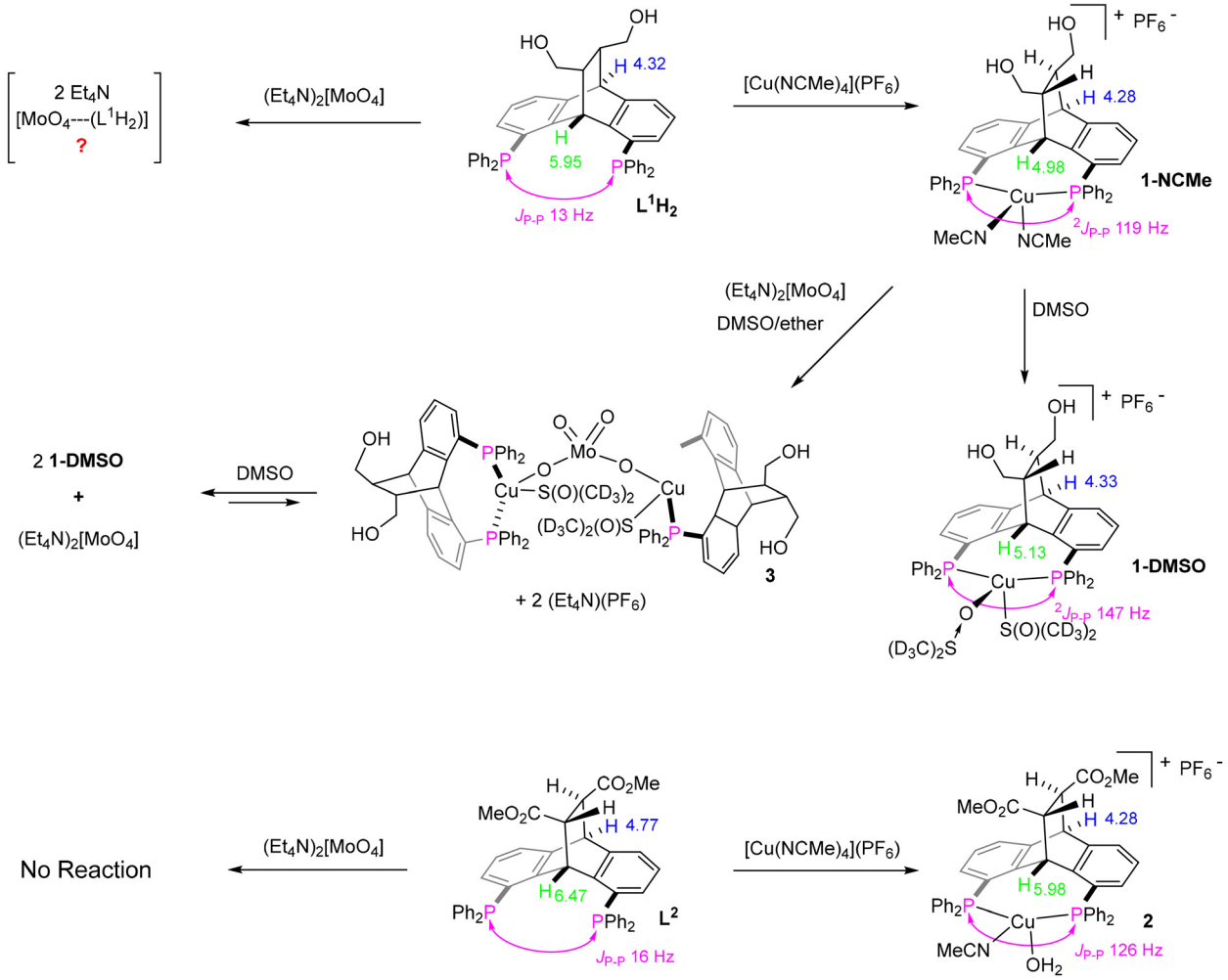

Scheme 1 Synthesis of L^1H_2 and L^2 complexes described in this work.

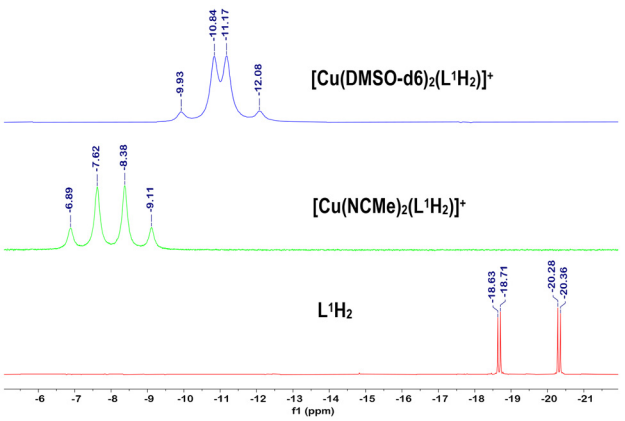

Fig. 2 ^{31}P $\{^1H\}$ NMR spectra obtained for L^1H_2 (red, bottom), **1**-NCMe (green, middle), and **1**-DMSO (blue, top).

nates both phosphorus donors. Related large $^2J_{P-P}$ values resulting from coupling through bonds to metals have been reported.[38–40]

To further characterize **1**-NCMe, and to rule out the contribution of ^{63}Cu ($I = 3/2$) to the coupling observed above, we pursued ^{63}Cu NMR spectroscopy.[41] No signal was observed at room temperature in CD_2Cl_2 solution after several hours. Furthermore, the complex was found to precipitate from concentrated solutions of CD_2Cl_2 upon prolonged data collection. As the complex demonstrated comparable or higher solubility in acetonitrile, and the concentrated solution of $[Cu(NCMe)_4](PF_6)$ in CD_3CN (~0.2 mM) gave a good ^{63}Cu NMR signal, we turned to CD_3CN. Notably, the ^{31}P $\{^1H\}$ NMR spectrum of **1**-NCMe in CD_3CN contains one broad peak ($\Delta\upsilon_{\frac{1}{2}}$ ~ 400 Hz at 15 °C and below this temperature, see SI), as opposed to the well-defined AB pattern in CD_2Cl_2. The peak becomes broader above 15 °C ($\Delta\upsilon_{\frac{1}{2}}$ ~ 700 Hz at 60 °C). Consistent with these findings, we were able to observe a broad ^{63}Cu NMR peak at 15 °C ($\Delta\upsilon_{\frac{1}{2}}$ ~ 1030 Hz) at 20 ppm (*vs.* $[Cu(NCMe)_4](PF_6)$). The signal becomes somewhat narrower below this temperature, while shifting slightly downfield (Fig. 3). In contrast, the ^{63}Cu signal becomes broader at 30 °C, and disappears entirely above this temperature.

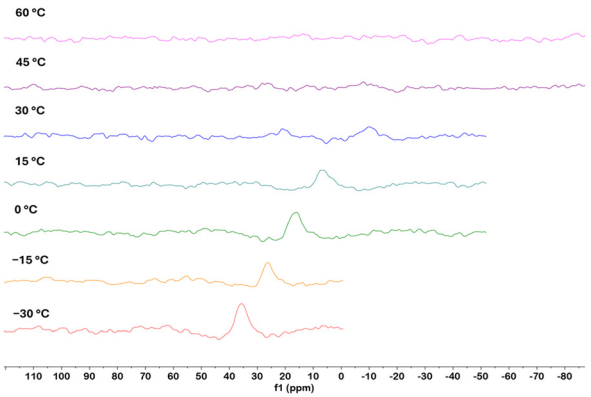

Fig. 3 ^{63}Cu NMR spectra (CD_3CN) of **1**-NCMe at the temperatures denoted.

Our multiple attempts to obtain X-ray quality crystals of **1**-NCMe from CH_3CN/ether were not successful, forming microcrystalline solid instead. Thus, the product was recrystallized from DMSO-d_6/ether, yielding pale yellow crystals. **1**-DMSO demonstrates similar spectral features to **1**-NCMe, including a significant upfield shift of the bridgehead proton facing Cu(I), and an AB pattern in ^{31}P $\{^1$H$\}$ NMR ($^2J_{P-P}$ = 147 Hz, $\Delta\upsilon$ = 201 Hz). X-ray structure determination revealed the structure of $[Cu(DMSO\text{-}d_6)_2(L^1H_2)](PF_6)$ (**1**-DMSO); the structure is shown in Fig. 4. Cu(I) adopts a distorted tetrahedral geometry, coordinated by $\mathbf{L^1H_2}$ (P–Cu–P angle of 123.1(1)°) and two DMSO ligands. The DMSO ligands exhibit linkage isomerism, with one coordinating through oxygen (O-DMSO) and the other through sulfur (S-DMSO). Notably, the diol functionality in the back of the ligand appears predisposed to coordinate another metal.

To obtain additional insight into the Cu(I) chemistry of dibenzobarrelene ligands, we also investigated coordination chemistry of the diester ligand $\mathbf{L^2}$. While no reactivity with Mo (VI) is expected for $\mathbf{L^2}$, it is expected to demonstrate similar chemistry with Cu(I). The reaction of $\mathbf{L^2}$ with $[Cu(NCMe)_4](PF_6)$ formed a pale yellow-brown solution, from which the product **2**-NCMe was isolated in high yield. The complex was characterized by ^{1}H, ^{13}C $\{^1$H$\}$, and ^{31}P $\{^1$H$\}$ NMR spectroscopy, and HRMS. The HRMS contains the molecular ion at m/z = 753.1362, consistent with $[Cu(L^2)]^+$ (m/z = 753.1385). The ^{1}H NMR spectrum of **2**-NCMe (CD_2Cl_2) demonstrates a significant upfield shift for the metal-facing bridgehead proton (5.98 ppm in **2**-NCMe *vs.* 6.47 ppm in $\mathbf{L^2}$), whereas the second bridgehead proton is again barely affected (4.84 ppm in **2**-NCMe *vs.* 4.77 ppm in $\mathbf{L^2}$). The ^{1}H NMR suggests a single acetonitrile ligand coordinated to the metal, consistent with the X-ray structure (Fig. 5). The ^{31}P $\{^1$H$\}$ spectrum demonstrates an AB pattern, with a similar $^2J_{P-P}$ value (126 Hz).

2-NCMe can be crystallized from acetonitrile/ether to afford nearly colorless blocks. The X-ray structure determination revealed the $[Cu(L^2)(NCMe)(L)](PF_6)$ composition (Fig. 5), with Cu(I) displaying distorted tetrahedral geometry. As suggested by ^{1}H NMR, only one acetonitrile binds to the metal. There is a minor occupancy disorder at the fourth coordination position L, with L being 75% OH_2 and 25% THF. $\mathbf{L^2}$ demonstrates a

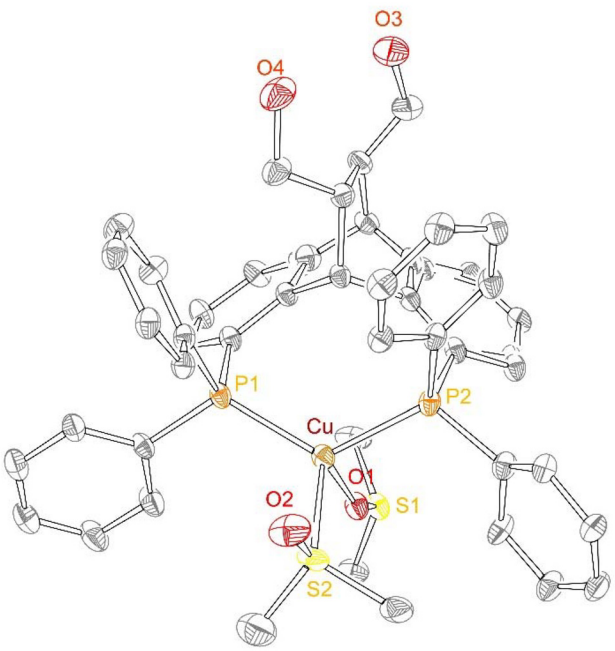

Fig. 4 X-ray structure (ORTEP rendering, 40% probability) of **1**-DMSO. Hydrogen atoms, alternative conformations of one of DMSO ligands, some of the phenyl rings, and the diol are omitted for clarity. Selected bond distances (Å) and angles (°): Cu–P1 2.2558(5), Cu–P2 2.2740(5), P1–Cu1–P2 123.13(2).

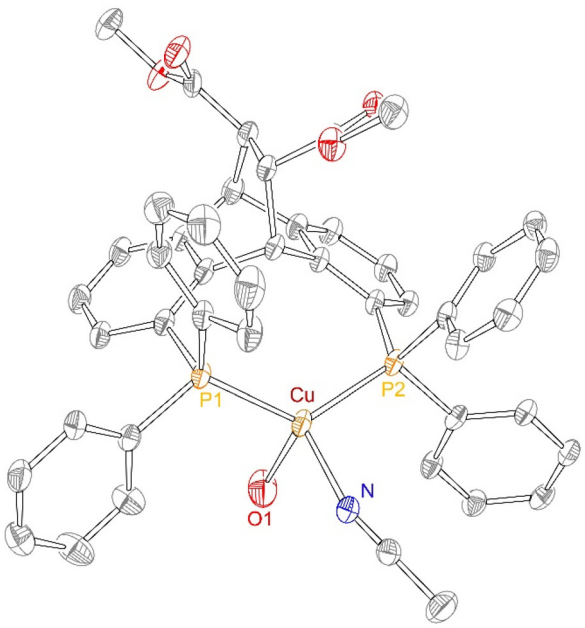

Fig. 5 X-ray structure (ORTEP rendering, 40% probability) of **2**. H atoms, PF_6 counterion, and co-crystallized solvents are omitted for clarity. Selected bond distances (Å) and angles (°): Cu–P1 2.268(1), Cu–P2 2.243(1), P2–Cu1–P1 124.87(5).

very similar coordination environment to $\mathbf{L^1H_2}$. Thus, P–Cu–P angle is 124.9(1) ° (123.1(1) ° for **1**-DMSO); the bridgehead H is 2.86 Å away from Cu (2.90 Å in **1**-DMSO).

Reactions of the ligand precursors with $[MoO_4]^{2-}$

Following the investigation of the chemistry of $\mathbf{L^1H_2}$ and $\mathbf{L^2}$ with Cu(I), their reactivity with $[MoO_4]^{2-}$ was investigated. Unsurprisingly, no complex formation takes place between $\mathbf{L^2}$ and Mo(VI), based on the NMR spectroscopic data. However, the NMR spectroscopic and mass spectrometric characterization of the reaction between $\mathbf{L^1H_2}$ and $(Et_4N)_2[MoO_4]$ proved less conclusive, and no X-ray quality crystals were obtained. The ^{1}H NMR spectrum demonstrates some changes in the chemical shift of the ligand protons which could be consistent with the formation of new species. Of the two bridgehead protons, a slight shift is observed for the bridgehead proton further away from the phosphine groups (4.53 ppm for the reaction product *vs.* 4.32 ppm for $\mathbf{L^1H_2}$). However, no change is observed for the bridgehead proton at 5.95 ppm. A similar situation is observed for the protons in the α- and β-positions to the alkoxide groups: while some protons demonstrate slight changes in their chemical shifts, other protons remain in their positions. The ^{31}P $\{^1H\}$ NMR spectrum contains two doublets at −19.27 ppm and −21.17 ppm, with J_{P-P} = 13 Hz. These values are close to the corresponding values of the free ligand (−18.67 and −20.32 ppm, J_{P-P} = 13 Hz). Most importantly, repeated attempts to observe the postulated species "$[MoO_3(L^1)]^{2-}$" in HRMS (ESI^-) were not successful. Instead, we observed peaks corresponding to free ligand (m/z = 635.2255, ESI^+) and $[MoO_3(OH)]^-$ (m/z = 162.8936, ESI^-). Additional Mo(VI)-based peaks were observed well below the expected peak for "$[MoO_3(L^1)]$". We note that, in the absence of definitive crystal structures, HRMS previously served as an indispensable technique to confirm the formation of various $[MoO_3(L)]^{2-}$ complexes with catecholate ligands. Therefore, the above data suggests that a well-defined complex between L^1 and Mo(VI) does not form.

To further investigate this issue, we turned to DFT calculations. $[MoO_3(L^1)]^{2-}$ is a well-defined minimum as shown in Fig. 6. The Mo(VI) ion adopts a structure intermediate between square pyramidal and trigonal bipyramidal, as evidenced by τ_5 = 0.52.[42] This is in contrast to our previous catecholate complexes that typically had $\tau_5 \sim 0$ and were best described as basally distorted square pyramid.[15,16,18,43] The reaction of $[MoO_4]^{2-}$ and $\mathbf{L^1H_2}$ to form H_2O and $[MoO_3(L^1)]^{2-}$ is calculated to be endergonic by 13.3 kcal mol^{-1}. This surprised us because catechol is well known to form a similar structure in our earlier attempts to make mixed Mo(VI)/Cu(I) heterodinuclear complexes.[15,16,18] The reaction of $[MoO_4]^{2-}$ and catechol to form H_2O and $[(catecholate)MoO_3]^{2-}$ is exergonic by 13.8 kcal mol^{-1}. While diol is less acidic and therefore should have a more endergonic formation than catechol ($pK_{a,1} \sim pK_{a,2} \sim 17$ for a diol *vs.* $pK_{a,1}$ = 9.3 and $pK_{a,2}$ = 13.0 for catechol),[44] this acidity difference does not explain the ∼30 kcal mol^{-1} calculated difference in free energy changes for these two ligands binding Mo(VI). We computationally simplified $\mathbf{L^1H_2}$ to the bridgehead of the dibenzobarrelene , 1,4-butanediol, and the analogous reaction to form $[(1,4\text{-butanediolate})MoO_3]^{2-}$ is endergonic by 13.4 kcal mol^{-1}; nearly identical to $\mathbf{L^1H_2}$. Noting that Mo forms a seven-membered metallacycle in $[MoO_3(L^1)]^{2-}$ and a five-membered metallacycle in the catecholate complex, we also investigated the reaction with 1,2-ethanediol. This reaction to form $[(1,2\text{-ethanediolate})MoO_3]^{2-}$ is slightly endergonic at 4.5 kcal mol^{-1} and more consistent with the pK_a differences between the ligands. Within the error of DFT and ligand simplification, these findings suggest modification of the bridgehead diol may allow for the desired ligation of Mo(VI) in a next-generation ligand design.

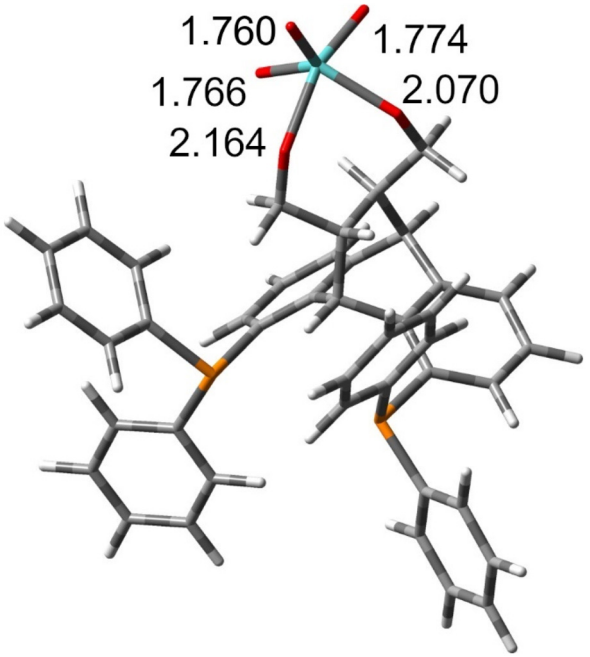

Fig. 6 Optimized structure of putative $[MoO_3(L^1)]^{2-}$ with Mo–O bond lengths listed (Å). The O–Mo–O angles are 130.5° and 161.5°.

Reactivity of Cu(I) complex of L^1H_2 with $[MoO_4]^{2-}$: formation and characterization of heterobimetallic product

As the direct incorporation of $[Mo^{VI}O_3]$ was not successful, we pursued the reaction of Cu(I) complex **1**-NCMe with molybdate. Treatment of the acetonitrile solution of $(Et_4N)_2[MoO_4]$ with the dichloromethane solution of $[Cu(NCMe)_2(L^1H_2)](PF_6)$ results in the formation of heterogeneous solution, from which white solid can be isolated. The resulting white solid was found to be insoluble in acetonitrile, tetrahydrofuran, or dichloromethane. However, it was partially soluble in DMSO-d_6, forming a yellow solution. Crystallization from DMSO/ether leads to the formation of yellow crystals. X-ray structure determination reveals the structure of pseudo-C_2-symmetric heterotrinuclear complex $[MoO_2(\mu_2\text{-}O)_2\{Cu(DMSO\text{-}d_6)(L^1H_2)\}_2]$ (**3**), in which the central molybdate interacts with two copper(I) centers *via* a single bridging oxo bond to each, $[Cu^I–O–Mo^{VI}(O_2)–O–Cu^I]$. As the structure exhibited significant twin-

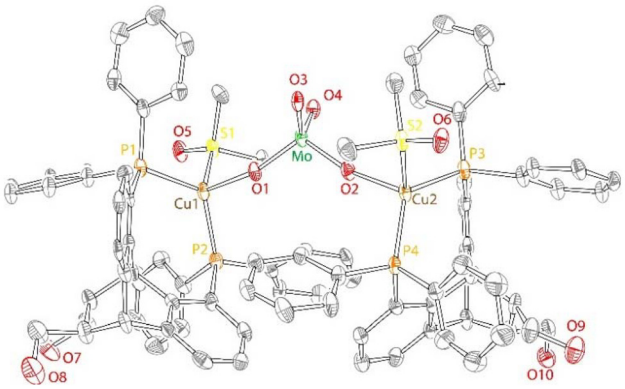

Fig. 7 X-ray structure (ORTEP rendering, 30% probability) of **3**. Alternative positions of several oxygen atoms and phenyl rings, H atoms, and co-crystallized solvents are omitted for clarity. Selected bond distances (Å) and angles (°): Mo–O1 1.77(5), Mo–O2 1.79(1), Mo–O3 1.75(2), Mo–O4 1.75(2), Cu1–P1 2.274(3), Cu1–P2 2.273(3), Cu2–P3 2.274(3), Cu2–P4 2.275(3), P2–Cu1–P1 124.2(1), P3–Cu2–P4 123.6(1), Mo–O1 Cu1 138(4), Mo–O2–Cu2 161.9(4).

ning and the ensuing disorder, individual bond distances and angles will not be discussed (selected metrics are presented in Fig. 7). While there are examples in the literature of the discrete complexes bearing related {$MoCu_2$} trimetallic core,[26,28,29] they all appear to contain Cu(II). We note that polymeric species containing {Mo(VI)–O–Cu(I)}–O repeating structural units have been previously reported.[27,30] We propose that the initial reaction of **1**-NCMe with one equivalent of molybdate forms oligo- or polymeric insoluble structures with a recurring {O–Cu[L^1]–O–MoO_2–} motif. This structure is broken by DMSO, stabilizing complex **3** in a discrete, molecular form.

Following the stoichiometry observed in **3**, we also investigated the reaction of two equivalents of $[Cu(NCMe)_2(L^1H_2)]^+$ with one equivalent of $[MoO_4]^{2-}$. Mixing $(Et_4N)_2[MoO_4]$ with two $\mathbf{L^1H_2}$ and two $[Cu(NCMe)_4](PF_6)$ in acetonitrile/THF forms a partially heterogeneous solution. The product of the reaction is only slightly soluble in dichloromethane but fully soluble in DMSO-d_6 (yellow solution). ^{1}H NMR of the crude product demonstrates a single species consistent with a single type of $\mathbf{L^1H_2}$ environment (Fig. S36). However, this proton NMR is also remarkably similar to the spectrum of **1**-DMSO taken in DMSO-d_6 (Fig. S37). Furthermore, the NMR spectrum contains peaks representative of tetraethylammonium protons. Only a slight difference is observed between the ^{31}P NMR of **1**-DMSO (in DMSO) and tentative "**3**". We propose that, while forming a discrete trimer in the solid state, complex **3** exists in DMSO solution in equilibrium with **1**-DMSO and molybdate (Scheme 1). In further support of this hypothesis, HRMS spectrum of the crude product demonstrates the presence of molybdate (m/z = 162.8963; calculated m/z = 162.8929 for $[MoO_3OH]^{1-}$) and $[Mo_2O_7]$ ion (m/z of 305.7840 for the singly charged and 150.8888 for the doubly charge ion) in the negative mode. Our multiple attempts to obtain tetraethylammonium-free samples of **3** were unsuccessful, suggesting that **3** co-crystallizes with molybdate or tetraethylammonium hexafluorophosphate.

Summary and conclusions

In conclusion, our study demonstrated that dibenzobarrelene ligand framework can lead to the heterobimetallic Mo(VI)/Cu(I) complexes, albeit not in the way originally postulated. Specifically, $\mathbf{L^1H_2}$ was found to coordinate Cu(I) *via* the diphosphine chelate, but the diol(ate) chelate failed to produce well-defined Mo(VI) complexes. However, $[Mo^{VI}O_4]^{2-}$ was found to coordinate $[Cu(L^1H_2)]^+$ species directly, through the formation of Mo–O–Cu bonds. The resulting heterobimetallic species, although metastable, is a promising candidate for CO/CNR reactivity studies: (1) it features nucleophilic Mo(VI)-oxo and Cu(I) in close proximity and (2) Cu(I) should be able to coordinate a substrate at the position occupied by labile NCMe or DMSO ligands. In future studies, we will explore several additional avenues in this chemistry, including (1) reactivity of the synthesized heterobimetallic complex with CO/CNR; (2) investigation of partially sulfidated Mo(VI) precursors (such as $[MoO_3S]^{2-}$ and $[MoO_2S_2]^{2-}$) to form sulfido-bridged heterodinuclear complexes; and (3) additional dibenzobarrelene ligands which contain better chelating or more acidic functionalities to coordinate Mo(VI).

Experimental

General

All reactions involving air-sensitive materials were carried out in a nitrogen-filled glovebox. 1,8-Bis(diphenylphosphaneyl)-9,10-dihydro-9,10-ethanoanthracene-11,12-diyldimethanol ($\mathbf{L^1H_2}$ ligand) and 9,10-ethanoanthracene-11,12-dicarboxylic acid, 1,8-bis(diphenylphosphino)-9,10-dihydro-,11,12-dimethyl ester ($\mathbf{L^2}$ ligand) were synthesized by the Gelman group at the Hebrew University of Jerusalem. Tetrakis(acetonitrile)copper(I) hexafluorophosphate was purchased from Sigma and used as received. All non-deuterated solvents were purchased from Aldrich and were of HPLC grade. The non-deuterated solvents were purified using an MBraun solvent purification system. Dichloromethane-d_2, dimethylsulfoxide-d_6 and acetonitrile-d_3 were purchased from Cambridge Isotope Laboratories. All solvents were stored over 3 Å molecular sieves. Compounds were routinely characterized by ^{1}H, ^{31}P, and ^{13}C NMR spectroscopy (including 2D techniques such as ^{1}H–^{1}H COSY, HSQC, and ROESY) and high-resolution mass spectrometry. Selected compounds were characterized by X-ray crystallography and ^{63}Cu NMR spectroscopy. Ligands and metal complexes characterization were carried out at the Lumigen Instrument Center at Wayne State University. NMR spectra of the ligands and metal complexes were recorded on an Agilent DD2-600 MHz Spectrometer, and an Agilent 400 MHz Spectrometer in CD_2Cl_2 at room temperature or CD_3CN at various temperatures (−30 °C to 60 °C). Chemical shifts and coupling constants (J)

were reported in parts per million (δ) and Hertz respectively. Detailed assignments of the signals in ^{1}H NMR are given in the SI. High resolution mass spectra of the metal complexes (unless otherwise stated) were collected on a Thermofisher Scientific LTQ Orbittrap XL mass spectrometer. The MS survey scan was set from 200–2000. The resolution was set to 60 000. In all cases, only one microscan was used in the analysis. HRMS for ligand run using a LCT Premier XE with a range of 200–2000 scans. Leucine Enkephalin was used as a lockmass.

Synthesis and characterization of ligands and metal complexes

L^1H_2. Synthesis and characterization of **L^1H_2** in $CDCl_3$ has been previously reported.[31] The spectroscopic characterization of **L^1H_2** in CD_2Cl_2 is provided below. ^{1}H NMR (400 MHz, CD_2Cl_2) δ 7.40–7.15 (m, 20 H), 7.06 (m, 4H), 6.91 (dd, J_1 = 8 Hz, J_2 = 4 Hz, 1H), 6.75 (dd, J_1 = 8 Hz, J_2 = 4 Hz, 1H), 5.95 (s, 1H, bridgehead C*H*), 4.32 (s, 1H, bridgehead C*H*), 3.23 (dd, J_1 = J_2 = 8 Hz, 1H), 3.07 (dd, J_1 = J_2 = 8 Hz, 1H), 2.90 (m, 2H), 1.76 (br s, 2H, O*H*), 1.53 (m, 1H), 1.17 (m, 1H). ^{31}P NMR (CD_2Cl_2, 162 MHz) δ −18.67 (d, J_{P-P} = 13 Hz), −20.32 (d, J_{P-P} = 13 Hz). ^{13}C {^{1}H} NMR {^{1}H} (101 MHz, CD_2Cl_2) δ 147.57, 147.28, 146.35, 146.04, 143.96 (d, J = 7 Hz), 141.21 (d, J = 6 Hz), 137.58, 137.48, 137.14, 137.05, 136.97, 136.84 (t, J = 4 Hz), 134.17, 134.00 (d, J = 7 Hz), 133.76 (d, J = 5 Hz), 133.68, 133.60, 133.49, 133.20 (d, J = 11 Hz), 132.56 (d, J = 14 Hz), 131.12, 130.47, 128.72 (d, J = 4 Hz), 128.51, 128.47, 128.44, 128.42, 128.40, 128.34, 128.28, 128.22, 126.15, 125.71, 124.28, 65.66 (d, J = 12 Hz), 46.67, 45.32 (d, J = 11 Hz), 41.22 (t, J = 23 Hz), 29.65, 15.05.

L^2. 1,8-Bis-(diphenylphosphino)anthracene (2 g, 3.6 mmol) and dimethyl fumarate (5.27 g, 36 mmol) were refluxed in 40 ml of xylene under nitrogen. The solution was allowed to cool to room temperature and the remaining solid was filtered. The filtrate was evaporated, and methanol was added to precipitate the crude product. The white solid was filtered, washed with a small amount of the same solvent and dried in vacuum affording 1.6 g (64%) of the desired product. ^{1}H NMR (400 MHz, $CDCl_3$) δ 7.29–6.88 (m, 24H), 6.78 (dd, J = 8, 3 Hz, 1H), 6.61 (dd, J = 8, 3 Hz, 1H), 6.42 (s, 1H), 4.68 (s, 1H), 3.55 (s, 3H), 3.35 (dd, J = 5, 3 Hz, 1H), 3.02 (s, 3H), 2.87 (dd, J = 7, 1 Hz, 1H). ^{31}P {^{1}H} NMR (162 MHz, $CDCl_3$) δ −17.63 (d, J_{P-P} = 15 Hz), −21.03 (d, J_{P-P} = 16 Hz). ^{1}H NMR (400 MHz, CD_2Cl_2) δ 7.38–7.02 (24 H), 6.86 (br s, 1H), 6.70 (br s, 1H), 6.47 (br s, 1H, bridgehead-H), 4.77 (br s, 1H, bridgehead-H), 3.61 (s, 3H, CO_2CH_3), 3.38 (br s, 1H, MeO_2CCCH), 3.12 (s, 3H, CO_2CH_3), 2.94 (br s, 1H, MeO_2CCCH). ^{13}C {^{1}H} NMR (101 MHz, CD_2Cl_2) δ 173.03, 172.83, 147.13, 146.85, 146.56, 146.24, 143.08 (d, J = 7 Hz), 141.27 (d, J = 5 Hz), 138.59 (d, J = 12 Hz), 138.16 (d, J = 11 Hz), 137.66 (d, J = 11 Hz), 136.96 (d, J = 12 Hz), 134.68, 134.45 (d, J = 4 Hz), 134.23, 134.10 (d, J = 1 Hz), 138.90 (d, J = 2 Hz), 138.82, 133.69, 133.64, 133.55, 133.50, 133.03 (d, J = 3 Hz), 131.15, 129.24, 128.99, 128.91 (d, J = 2 Hz), 128.84, 128.78, 128.74, 128.67, 128.62, 126.90, 126.73, 125.78, 125.21, 52.47, 51.97, 47.63, 46.75, 42.78 (t, J = 23 Hz).

$[Cu(NCMe)_2(L^1H_2)](PF_6)$ (1-NCMe). $[Cu(NCMe)_4](PF_6)$ (12 mg, 0.032 mmol, 1.0 equiv.) was dissolved in acetonitrile (2 mL) and **L^1H_2** (20 mg, 0.032 mmol, 1.0 equiv.) was dissolved in dichloromethane (2 mL). Both solutions were cooled to −33 °C. The colorless solution of **L^1H_2** was then added dropwise to a stirred colorless solution of $[Cu(NCMe)_4](PF_6)$ producing a transparent pale-yellow solution. The reaction mixture was stirred for 1 h, after which volatiles were removed *in vacuo*. This solid can be recrystallized *via* vapor diffusion using acetonitrile and ether (22 mg, 0.024 mmol, 75%). ^{1}H NMR (CD_2Cl_2, 400 MHz) δ 7.49 (m, 18H), 7.40 (m, 4H), 7.09 (m, 2H), 6.70 (t, J = 8 Hz, 1H), 6.57 (t, J = 8 Hz, 1H), 4.98 (s, 1H, bridgehead C*H*), 4.28 (s, 1H, bridgehead C*H*), 3.25 (dd, $^2J_{H-H}$ = 10 Hz, $^3J_{H-H}$ = 8 Hz, 1H, C*H*H), 2.88 (dd, $^2J_{H-H}$ = $^3J_{H-H}$ = 8 Hz, 1H, CH*H*), 2.26 (dd, $^2J_{H-H}$ = $^3J_{H-H}$ = 8 Hz, 1H, CH*H*), 1.87 (s, 6H, CH_3CN), 1.73 (m + m, 2H, CH + C*H*H), 1.01 (m, 1H, C*H*). ^{31}P {^{1}H} NMR (162 MHz, CD_2Cl_2, 288 K) δ −7.19 (d, $^2J_{P-P}$ = 119 Hz), −8.82 (d, $^2J_{P-P}$ = 119 Hz). ^{31}P NMR (242 MHz, CD_3CN, 288 K) δ −7.19 (br s, $\Delta\upsilon_{1/2}$ = 400 Hz). ^{13}C {^{1}H} NMR (101 MHz, CD_2Cl_2) δ 148.09, 147.92, 145.89, 145.82, 145.71, 142.45 (d, J = 7 Hz), 135.44 (d, J = 16 Hz), 134.77 (dd, J1 = 17 Hz, J2 = 1 Hz), 134.69 (d, J = 1 Hz), 134.26 (d, J = 1 Hz), 134.10, 133.96, 132.46 (d, J = 1 Hz), 131.85 (d, J = 1 Hz), 131.59 (d, J = 1 Hz), 131.14 (d, J = 1 Hz), 130.82 (d, J = 1 Hz), 130.48 (d, J = 1 Hz), 130.07 (d, J = 1 Hz), 129.99 (d, J = 1 Hz), 129.87, 129.77, 129.67 (d, J = 4.0 Hz), 129.59 (d, J = 4.0 Hz), 129.53, 129.50, 129.30, 129.21, 128.26 (d, J = 1 Hz), 127.74, 127.71, 127.00 (d, J = 6 Hz), 126.80 (d, J = 6 Hz), 126.48 (d, J = 1 Hz), 125.41, 125.07, 119.51, 66.65, 65.29, 46.84, 45.18, 44.48, 42.33 (t, $^3J_{C-P}$ = 15 Hz, bridgehead C), 2.23. ^{63}Cu NMR (159.03 MHz, CH_3CN, 288 K) δ 7 (br s, $\Delta\upsilon_{1/2}$ = 1100 Hz). ^{63}Cu NMR (159.03 MHz, CH_3CN, 243 K) δ 35 (br s, $\Delta\upsilon_{1/2}$ = 900 Hz). HRMS (ESI$^+$) m/z 697.1434 (calculated m/z for $[Cu(L^1H_2)]^+$ 697.1434).

$[Cu(DMSO\text{-}d_6)_2(L^1H_2)](PF_6)$ (1-DMSO). $[Cu(NCMe)_2(L^1H_2)](PF_6)$ (**1**-NCMe) (46 mg, 0.050 mmol) was dissolved in DMSO-d_6 (1 mL). The DMSO-d_6 solution was subjected to vapor diffusion of ether in course of 3 days, producing pale-yellow crystals of **1**-DMSO (37 mg, 0.042 mol, 84% yield). ^{1}H NMR (400 MHz, CD_2Cl_2) δ 7.70–7.40 (m, 20H), 7.37 (d, $^3J_{H-H}$ = 7 Hz, 2H), 7.10 (q, $^3J_{H-H}$ = 7 Hz, 2H), 6.75 (t, $^3J_{H-H}$ = 7 Hz, 1H), 6.63 (t, $^3J_{H-H}$ = 7 Hz, 1H), 5.13 (s, 1H), 4.33 (s, 1H), 3.06 (s, 2H), 2.24 (t, $^3J_{H-H}$ = 8 Hz, 1H), 1.74 (s, 2H), 1.03 (s, 1H). ^{31}P {^{1}H} NMR (162 MHz, CD_2Cl_2) δ −10.26 (d, $^2J_{P-P}$ = 147 Hz), −11.79 (d, J = 147 Hz). ^{13}C {^{1}H} NMR {^{1}H} (CD_2Cl_2, 101 MHz) δ 147.84, 147.65, 145.64, 145.57, 145.35 (d, J = 4 Hz), 142.20 (d, J = 6 Hz), 135.0 (dd, J = 14 Hz, 3.0 Hz), 134.65 (dd, J = 13, 3 Hz), 134.05 (dd, J = 13, 3 Hz), 133.55 (dd, J = 13, 3 Hz), 131.71, 131.09 (d, J = 3 Hz), 130.85 (d, J = 5 Hz), 130.72, 130.24 (d, J = 5 Hz), 130.01 (d, J = 6 Hz), 129.94, 129.77, 129.66, 129.46, 129.39, 129.26, 129.21, 129.14, 129.05, 127.98 (d, J = 4 Hz), 127.74, 126.45 (d, J = 4 Hz), 126.26 (d, J = 5 Hz), 125.88, 125.58 (d, J = 5 Hz), 125.28 (d, J = 5 Hz), 66.04, 65.61, 64.87, 46.52, 45.11, 44.24, 42.06 (t, $^3J_{C-P}$ = 16 Hz, bridgehead C), 15.06. ^{1}H NMR (400 MHz, DMSO-d6) δ 7.45–7.40 (m, 20H), 7.13 (m, 2H), 6.62 (br s, 2H), 6.47 (br s, 1H), 4.74 (t, J = 4 Hz, 1H), 4.73 (s, 1H, bridgehead-H), 3.98 (t, J = 4 Hz, 1H), 3.23 (quint, J = 4 Hz, 1H), 2.63 (td, J = 8.0 Hz, 4.0 Hz, 1H), 1.80 (m, 1H), 1.72 (m, 1H), 1.34 (m, 1H), 0.64 (m, 1H).

$[Cu(NCMe)(OH_2)(L^2)](PF_6)$ (2-NCMe). A colorless solution of tetrakis(acetonitrile)copper(I) hexafluorophosphate

$[Cu(NCMe)_4](PF_6)$ (8.0 mg, 0.023 mmol, 1 equiv.) in acetonitrile (2 mL) and a colorless solution of $\mathbf{L^2}$ (16.0 mg, 0.023 mmol, 1.0 equiv.) in dichloromethane (2 mL) were prepared and cooled to −33 °C. The solution of cold $\mathbf{L^2}$ was then added dropwise to a stirring solution of cold $[Cu(NCMe)_4](PF_6)$ producing a transparent pale brown solution. The reaction mixture was stirred for 1 hour, upon which volatiles were removed *in vacuo.* The product was obtained as a white color solid (96%). ^{1}H NMR (600 MHz, CD_2Cl_2) δ 7.70–7.35 (20H, Ar–*H*), 7.14 (m, 4H, Ar–*H*), 6.78 (m, 1H, Ar–*H*), 6.70 (m, 1H, Ar–*H*), 5.98 (br s, 1H, bridgehead-C*H*), 4.84 (s, 1H, bridgehead-C*H*), 3.66 (s, 3H, OCH_3), 3.40 (br s, 1H, C*H*), 2.69 (br s, 1H, C*H*), 2.52 (s, 3H, OCH_3). ^{31}P {^{1}H} NMR (243 MHz, CD_2Cl_2) δ −8.60 (d, $^2J_{P-P}$ = 125 Hz), −12.04 (d, $^2J_{P-P}$ = 125 Hz). ^{13}C {^{1}H} NMR (CD_2Cl_2, 101 MHz) δ 172.73, 171.87, 147.76, 147.56, 146.21, 146.00, 144.37 (d, J = 8 Hz), 141.82 (d, J = 7 Hz), 134.70, 134.55, 134.41, 134.16 (d, J = 15 Hz), 133.70 (d, J = 14 Hz), 132.34 (d, J = 5 Hz), 132.16 (d, J = 1 Hz), 132.02 (d, J = 5 Hz), 131.66 (d, J = 2 Hz), 131.40 (d, J = 1 Hz), 131.32 (d, J = 2 Hz), 131.27, 130.94, 130.64 (d, J = 1 Hz), 130.57 (d, J = 2 Hz), 130.44 (d, J = 3 Hz), 130.26, 130.24, 130.21, 129.95, 129.85, 129.76, 129.69, 129.59, 129.30 (d, J = 9 Hz), 127.89 (d, J = 2 Hz), 127.23, 127.18, 127.14, 127.86 (d, J = 2 Hz), 126.82, 126.65, 126.31, 118.54, 66.03, 52.78, 51.72, 47.23, 46.84, 45.03, 42.58 (t, J = 18 Hz), 31.96, 23.03, 15.48, 14.26, 2.08. HRMS (ESI^+) m/z 753.1362 (calculated m/z for $[Cu(L^2)]^+$ 697.1385).

Reaction of $[MoO_4](Et_4N)_2$ with $\mathbf{L^1H_2}$. A 2 mL solution of tetraethylammonium molybdate $[MoO_4](Et_4N)_2$ (13.2 mg, 0.032 mmol, 1.0 equiv.) in acetonitrile and a 2 mL solution of $\mathbf{L^1H_2}$ (20.0 mg, 0.032 mmol, 1.0 equiv.) in dichloromethane were prepared and cooled to −33 °C. The solution of cold L^7 was then added dropwise to a stirring solution of cold $[MoO_4](NEt_4)_2$ producing a pale pink solution. The reaction mixture was stirred for 1 hour, after which the volatiles were removed *in vacuo*. Reaction products were analyzed by ^{1}H and ^{31}P NMR spectroscopy and high-resolution mass spectrometry (see SI).

Reaction of $[MoO_4](Et_4N)_2$ and $\mathbf{L^2}$. A 2 mL solution of tetraethylammonium molybdate $[MoO_4](Et_4N)_2$ (12.0 mg, 0.029 mmol, 1.0 equiv.) in acetonitrile and a 2 mL solution of $\mathbf{L^2}$ (20.0 mg, 0.029 mmol, 1.0 equiv.) in dichloromethane were prepared and cooled to −33 °C. The solution of cold L^8 was then added dropwise to a stirring solution of cold $[MoO_4](NEt_4)_2$ producing a pale pink solution. The reaction mixture was stirred for 1 hour, after which the volatiles were removed *in vacuo*. The crude products of the reaction were analyzed by ^{1}H and ^{31}P NMR spectroscopy (see SI).

$[Cu_2(DMSO\text{-}d_6)_2(L^1H_2)_2MoO_4]$ (3). $[Cu(NCMe)_4](PF_6)$ (23 mg, 0.063 mmol) was dissolved in acetonitrile (2 mL) and $\mathbf{L^1H_2}$ (40 mg, 0.063 mmol) was dissolved in tetrahydrofuran (2 mL). Both solutions were cooled to −33 °C. The colorless solution of $\mathbf{L^1H_2}$ was then added dropwise to a stirred colorless solution of $[Cu(NCMe)_4](PF_6)$ producing a transparent pale-yellow solution. The reaction mixture was stirred for 1 h, after which volatiles were removed *in vacuo.* The resulting product ($[Cu(NCMe)_2(L^1H_2)](PF_6)$, **1**-NCMe) was dissolved in acetonitrile (2 mL). Tetraethylammonium molybdate $[MoO_4](Et_4N)_2$ (13.2 mg, 0.031 mmol, 0.5 equiv.) was also dissolved in acetonitrile (2 mL). Both solutions were cooled to −33 °C. The pale-yellow solution of **1**-NCMe was then added dropwise to a stirred colorless solution of $[MoO_4](Et_4N)_2$ producing a white cloudy solution. The reaction mixture was stirred for 1 h, after which volatiles were removed *in vacuo.* The addition of dichloromethane led to the separation of white precipitate. The liquid was decanted, and the solid was dried *in vacuo.* The resulting solid exhibited very low solubility in tetrahydrofuran, acetonitrile, or dichloromethane, but was soluble in dimethylsulfoxide (DMSO). Recrystallization from DMSO/ether *via* vapor diffusion yellow crystals of $[Cu_2(DMSO\text{-}d_6)_2(L^1H_2)_2MoO_4]$ (**3**, 52.7 mg, 0.030 mmol, 96%). The nature of the product was established by X-ray crystallography. ^{1}H and ^{31}P NMR of the product (in DMSO-d6) are nearly identical to the corresponding spectra of $[Cu(DMSO)_2(L^1H_2)](PF_6)$ (see SI for details).

Computational details

Geometry optimizations were performed in Gaussian 09[45] at the BP86[46,47]/def2-SVP[48] level of theory including solvation effects using SMD(MeCN).[49] Density fitting and ultrafine grids were employed. All minima were confirmed through harmonic frequency analysis and standard thermodynamic approximations were used to estimate Gibbs free energies at room temperature.[50] Single point energy refinements were performed in ORCA 6.0.1[51–53] at the BP86-D3BJ[54]/def2-TZVP/SMD (MeCN) and B3LYP[55–58]-D3BJ/def2-TZVP/SMD(MeCN) levels of theory using default numerical settings.[59–63] Approximate triple-zeta energies were calculated as $G_{TZ} = G_{DZ} - E_{DZ} + E_{TZ}$. Energies reported in the paper are the B3LYP refined triple-zeta free energies; all energies may be found in the SI. Electronic structure analyses and geometric analyses were performed in GaussView 6.0.[64] The XYZ coordinates for all optimized structures may be found in the SI.

Conflicts of interest

The are no conficts to declare.

Data availability

The data supporting this article have been included as part of SI. Supplementary information: NMR and mass spectra, X-ray collection and refinement details, computational details, and xyz structures for all optimized geometries. See DOI: **https://doi.org/10.1039/d5dt01337b**.

CCDC 2456598–2456600 contain the supplementary crystallographic data for this paper.[65a–c]

Acknowledgements

D. G., R. L. L., and S. G. acknowledge financial support from the US-Israel Binational Science Foundation (Grant

#2020129). S. G. and R. L. L. are grateful to the National Science Foundation (NSF) for current support through CHE-2348382. R. L. L. acknowledges NSF for computational resources through MRI CHE-1919571. Experimental characterization was carried out at Lumigen Instrument Center of Wayne State University. This work made use of the single-crystal XRD that was partially funded by the National Institutes of Health supplement grant #3R01EB027103-02S1.

References

1 A. C. Ghosh, C. Duboc and M. Gennari, Synergy between Metals for Small Molecule Activation: Enzymes and Bio-Inspired Complexes, *Coord. Chem. Rev.*, 2021, **428**, 213606, DOI: **10.1016/j.ccr.2020.213606**.

2 N. P. Mankad, Learning from Nature: Bio-Inspired Heterobinuclear Electrocatalysts for Selective CO_2 Reduction, *Trends Chem.*, 2021, **3**(3), 159–160, DOI: **10.1016/j.trechm.2020.12.002**.

3 B. G. Cooper, J. W. Napoline and C. M. Thomas, Catalytic Applications of Early/Late Heterobimetallic Complexes, *Catal. Rev.*, 2012, **54**(1), 1–40, DOI: **10.1080/01614940.2012.619931**.

4 E. Y. Tsui, J. S. Kanady and T. Agapie, Synthetic Cluster Models of Biological and Heterogeneous Manganese Catalysts for O_2 Evolution, *Inorg. Chem.*, 2013, **52**(24), 13833–13848, DOI: **10.1021/ic402236f**.

5 U. I. Kaluarachchige Don, C. A. M. Buddhika, G. Dmitri, R. L. Lord and S. Groysman, Design and Reactivity of Early-Late Bimetallics as Structural and Functional Models of Mo Cu CODH, *Comments Inorg. Chem.*, 2024, **44**(5), 349–384, DOI: **10.1080/02603594.2023.2298366**.

6 R. Hille, S. Dingwall and J. Wilcoxen, The Aerobic CO Dehydrogenase from *Oligotropha carboxidovorans*, *J. Biol. Inorg. Chem.*, 2015, **20**(2), 243–251, DOI: **10.1007/s00775-014-1188-4**.

7 H. Dobbek, L. Gremer, R. Kiefersauer, R. Huber and O. Meyer, Catalysis at a Dinuclear [CuSMo(O)OH] Cluster in a CO Dehydrogenase Resolved at 1.1 Å Resolution, *Proc. Natl. Acad. Sci. U. S. A.*, 2002, **99**(25), 15971–15976, DOI: **10.1073/pnas.212640899**.

8 N. P. Mankad and D. Ghosh, in 8.30 - Biomimetic Studies of the Mo/Cu Active Site of CO Dehydrogenase, *In Comprehensive Coord. Chem. III*, ed. E. Constable, G. Parkin and L. Que Jr, Elsevier, Oxford, 2021, 3rd edn, pp. 772–789. DOI: **10.1016/B978-0-08-102688-5.00060-X**.

9 C. Gourlay, D. J. Nielsen, J. M. White, S. Z. Knottenbelt, M. L. Kirk and C. G. Young, Paramagnetic Active Site Models for the Molybdenum–Copper Carbon Monoxide Dehydrogenase, *J. Am. Chem. Soc.*, 2006, **128**(7), 2164–2165, DOI: **10.1021/ja056500f**.

10 C. Gourlay, D. J. Nielsen, D. J. Evans, J. M. White and C. G. Young, Models for Aerobic Carbon Monoxide Dehydrogenase: Synthesis, Characterization and Reactivity of Paramagnetic $Mo^{V}O(\mu\text{-}S)CuI$ Complexes, *Chem. Sci.*, 2018, **9**(4), 876–888, DOI: **10.1039/C7SC04239F**.

11 D. Ghosh, S. Sinhababu, B. D. Santarsiero and N. P. Mankad, A W/Cu Synthetic Model for the Mo/Cu Cofactor of Aerobic CODH Indicates That Biochemical CO Oxidation Requires a Frustrated Lewis Acid/Base Pair, *J. Am. Chem. Soc.*, 2020, **142**(29), 12635–12642, DOI: **10.1021/jacs.0c03343**.

12 M. Takuma, Y. Ohki and K. Tatsumi, Sulfido-Bridged Dinuclear Molybdenum–Copper Complexes Related to the Active Site of CO Dehydrogenase: $[(Dithiolate)Mo(O)S_2Cu(SAr)]^{2-}$ (Dithiolate = $1,2\text{-}S_2C_6H_4$, $1,2\text{-}S_2C_6H_2\text{-}3,6\text{-}Cl_2$, $1,2\text{-}S_2C_2H_4$), *Inorg. Chem.*, 2005, **44**(17), 6034–6043, DOI: **10.1021/ic050294v**.

13 S. Groysman, A. Majumdar, S.-L. Zheng and R. H. Holm, Reactions of Monodithiolene Tungsten(VI) Sulfido Complexes with Copper(I) in Relation to the Structure of the Active Site of Carbon Monoxide Dehydrogenase, *Inorg. Chem.*, 2010, **49**(3), 1082–1089, DOI: **10.1021/ic902066m**.

14 A. Mouchfiq, T. K. Todorova, S. Dey, M. Fontecave and V. Mougel, A Bioinspired Molybdenum–Copper Molecular Catalyst for CO_2 Electroreduction, *Chem. Sci.*, 2020, **11**(21), 5503–5510, DOI: **10.1039/D0SC01045F**.

15 T. S. Hollingsworth, R. L. Hollingsworth, R. L. Lord and S. Groysman, Cooperative Bimetallic Reactivity of a Heterodinuclear Molybdenum–Copper Model of Mo–Cu CODH, *Dalton Trans.*, 2018, **47**(30), 10017–10024, DOI: **10.1039/C8DT02323A**.

16 U. I. Kaluarachchige Don, S. S. Kurup, T. S. Hollingsworth, C. L. Ward, R. L. Lord and S. Groysman, Synthesis and Cu(I)/Mo(VI) Reactivity of a Bifunctional Heterodinucleating Ligand on a Xanthene Platform, *Inorg. Chem.*, 2021, **60**(19), 14655–14666, DOI: **10.1021/acs.inorgchem.1c01735**.

17 U. I. Kaluarachchige Don, A. S. Almaat, C. L. Ward and S. Groysman, Studies Relevant to the Functional Model of Mo-Cu CODH: In Situ Reactions of Cu(I)-L Complexes with Mo(VI) and Synthesis of Stable Structurally Characterized Heterotetranuclear $Mo^{VI}{}_2Cu^{I}{}_2$ Complex, *Molecules*, 2023, **28**, 3644, DOI: **10.3390/molecules28083644**.

18 U. I. Kaluarachchige Don, Z. Palmer, C. L. Ward, R. L. Lord and S. Groysman, Combining $[Mo^{VI}O_3]$ and $[M^{0}(CO)_3]$ (M = Mo, Cr) Fragments within the Same Complex: Synthesis and Reactivity of the Single Oxo-Bridged Heterobimetallics Supported by Xanthene-Based Heterodinucleating Ligands, *Inorg. Chem.*, 2023, **62**(37), 15063–15075, DOI: **10.1021/acs.inorgchem.3c01929**.

19 N. Biswas, R. Mondal, K. U. Ansari, R. Yaseen, R. L. Lord, S. Groysman, D. Shimon and D. Gelman, High-Valent Nickel Complexes Supported by a Functionalized PC(sp^3)P Pincer Ligand: Properties and Catalysis, *Chem. – Eur. J.*, 2025, **31**(28), e202500618, DOI: **10.1002/chem.202500618**.

20 S. Mujahed, D. Gandolfo, L. Vaccaro, E. Kirillov and D. Gelman, A High-Valent Ru-PCP Pincer Catalyst for Hydrosilylation Reactions, *Mol. Catal.*, 2024, **553**, 113686, DOI: **10.1016/j.mcat.2023.113686**.

21 N. Biswas, P. Lönnecke, E. Kirillov and D. Gelman, Hydrogenation of CO_2 by a Tripodal Palladium Pincer

Complex, *ACS Catal.*, 2024, **14**(17), 13163–13173, DOI: 10.1021/acscatal.4c02523.

22 S. Gelman-Tropp, E. Kirillov, E. Hey-Hawkins and D. Gelman, Hydrogenation of CO_2 by a Bifunctional PC(sp^3)P Iridium(III) Pincer Complex Equipped with Tertiary Amine as a Functional Group, *Chem. – Eur. J.*, 2023, **29**(63), e202301915, DOI: 10.1002/chem.202301915.

23 S. De-Botton, S. Cohen and D. Gelman, Iridium PC(sp^3)P Pincer Complexes with Hemilabile Pendant Arms: Synthesis, Characterization, and Catalytic Activity, *Organometallics*, 2018, **37**(8), 1324–1330, DOI: 10.1021/acs.organomet.8b00105.

24 S. De-Botton, R. Romm, G. Bensoussan, M. Hitrik, S. Musa and D. Gelman, Coordination Versatility of P-Hydroquinone-Functionalized Dibenzobarrelene-Based PC(sp^3)P Pincer Ligands, *Dalton Trans.*, 2016, **45**(40), 16040–16046, DOI: 10.1039/C6DT02201D.

25 S. Musa, R. Romm, C. Azerraf, S. Kozuch and D. Gelman, New Possible Mode of Ligand–Metal Cooperation in PC(sp^3)P Pincer Complexes, *Dalton Trans.*, 2011, **40**(35), 8760–8763, DOI: 10.1039/C1DT10167F.

26 H. Oshio, T. Kikuchi and T. Ito, A Ferromagnetic Interaction between Cu^{2+} Centers through a $[CrO_4]^{2-}$ Bridge: Crystal Structures and Magnetic Properties of [{Cu(Acpa)}$_2$(μ-MO_4)] (M = Cr, Mo) (Hacpa = N-(1-Acetyl-2-Propyridene)(2-Pyridylmethyl)Amine), *Inorg. Chem.*, 1996, **35**(17), 4938–4941, DOI: 10.1021/ic960204+.

27 Z. Han, Y. Gao, X. Zhai and H. Song, A Copper–Organic Complex from Hydrothermal Reaction Involving in Situ Aromatic Nucleophilic Substitution of Ligand, *Inorg. Chem. Commun.*, 2007, **10**(9), 1079–1082, DOI: 10.1016/j.inoche.2007.05.022.

28 M.-L. Liu, G. Wen, M. Zhen-Ping, Z. Ping, G. Yue-Qiang and X. Liu, Syntheses, Crystal Structures and Magnetic Properties of Tungstato- and Molybdo-Bridged Dinuclear Copper(II) Complexes, *J. Coord. Chem.*, 2008, **61**(21), 3476–3485, DOI: 10.1080/00958970802068888.

29 H. I. Buvailo, V. G. Makhankova, V. N. Kokozay, I. V. Omelchenko, O. V. Shishkin, D. Matoga and J. Jezierska, Direct Synthesis of Heterometallic Cu/Mo Complexes with Aromatic Chelating N,N-Donating Ligands, *Inorg. Chim. Acta*, 2016, **443**, 36–44, DOI: 10.1016/j.ica.2015.12.019.

30 J.-D. Bai, Y.-H. Zhang, H. Shi, Q. Shi and F.-N. Shi, Synthesis, Structure and Lithium Storage Performance of a Copper–Molybdenum Complex Polymer Based on 4,4′-Bipyridine, *J. Solid State Chem.*, 2021, **298**, 122105, DOI: 10.1016/j.jssc.2021.122105.

31 S. Musa, I. Shaposhnikov, S. Cohen and D. Gelman, Ligand–Metal Cooperation in PCP Pincer Complexes: Rational Design and Catalytic Activity in Acceptorless Dehydrogenation of Alcohols, *Angew. Chem., Int. Ed.*, 2011, **50**(15), 3533–3537, DOI: 10.1002/anie.201007367.

32 C. Azerraf, A. Shpruhman and D. Gelman, Diels–Alder Cycloaddition as a New Approach toward Stable PC(sp^3)P-Metalated Compounds, *Chem. Commun.*, 2009, (4), 466–468, DOI: 10.1039/B815051F.

33 G. dos Passos Gomes, G. Xu, X. Zhu, L.-M. Chamoreau, O. Bistri-Aslanoff, S. Roland, I. V. Alagubin and M. Sollogoub, Mapping C–H···M Interactions in ConfinedSpaces:(α-ICyDMe)Au, Ag, Cu Complexes Reveal"Contra-Electrostatic H Bonds"Masquerading as Anagostic Interactions., *Chem. – Eur. J.*, 2021, **27**(31), 8127–8142, DOI: 10.1002/chem.202100263.

34 M. R. Hoffbauer, C. C. Comanescu, B. J. Dymm and V. M. Iluc, Influence of the Leaving Group on C–H Activation Pathways in Palladium Pincer Complexes, *Organometallics*, 2018, **37**(13), 2086–2094, DOI: 10.1021/acs.organomet.8b00237.

35 J.-C. Hierso, A. Fihri, V. V. Ivanov, B. Hanquet, N. Pirio, B. Donnadieu, B. Rebière, R. Amardeil and P. Meunier, "Through-Space" Nuclear Spin–Spin J_{PP} Coupling in Tetraphosphine Ferrocenyl Derivatives: A ^{31}P NMR and X-Ray Structure Correlation Study for Coordination Complexes, *J. Am. Chem. Soc.*, 2004, **126**(35), 11077–11087, DOI: 10.1021/ja048907a.

36 C. Azerraf, S. Cohen and D. Gelman, Roof-Shaped Halide-Bridged Bimetallic Complexes via Ring Expansion Reaction, *Inorg. Chem.*, 2006, **45**(17), 7010–7017, DOI: 10.1021/ic060700q.

37 O. Grossman, C. Azerraf and D. Gelman, Palladium Complexes Bearing Novel Strongly Bent Trans-Spanning Diphosphine Ligands: Synthesis, Characterization, and Catalytic Activity, *Organometallics*, 2006, **25**(2), 375–381, DOI: 10.1021/om050906j.

38 J.-C. Hierso, Indirect Nonbonded Nuclear Spin–Spin Coupling: A Guide for the Recognition and Understanding of "Through-Space" NMR *J* Constants in Small Organic, Organometallic, and Coordination Compounds, *Chem. Rev.*, 2014, **114**(9), 4838–4867, DOI: 10.1021/cr400330g.

39 B. A. Chalmers, P. S. Nejman, A. V. Llewellyn, A. M. Felaar, B. L. Griffiths, E. I. Portman, E.-J. L. Gordon, K. J. H. Fan, J. D. Woollins, M. Bühl, O. L. Malkina, D. B. Cordes, A. M. Z. Slawin and P. Kilian, A Study of Through-Space and Through-Bond J_{PP} Coupling in a Rigid Nonsymmetrical Bis(Phosphine) and Its Metal Complexes, *Inorg. Chem.*, 2018, **57**(6), 3387–3398, DOI: 10.1021/acs.inorgchem.8b00162.

40 T.-A. Nguyen, M.-J. Penouilh, H. Cattey, N. Pirio, P. Fleurat-Lessard, J.-C. Hierso and J. Roger, Unsymmetrically Substituted Bis(Phosphino)Ferrocenes Triggering Through-Space ^{31}(P, P′)-Nuclear Spin Couplings and Encapsulating Coinage Metal Cations, *Organometallics*, 2021, **40**(21), 3571–3584, DOI: 10.1021/acs.organomet.1c00465.

41 J. R. Black, W. Levason, M. D. Spicer and M. Webster, Synthesis and Solution Multinuclear Nuclear Magnetic Resonance Studies of Homoleptic Copper(I) Complexes of Group 15 Donor Ligands, *J. Chem. Soc., Dalton Trans.*, 1993, (20), 3129–3136, DOI: 10.1039/DT9930003129.

42 A. W. Addison, T. N. Rao, J. Reedijk, J. van Rijn and G. C. Verschoor, Synthesis, Structure, and Spectroscopic Properties of Copper(II) Compounds Containing Nitrogen–Sulphur Donor Ligands; the Crystal and Molecular

Structure of Aqua[1,7-Bis(N-Methylbenzimidazol-2′-yl)-2,6-Dithiaheptane]Copper(II) Perchlorate, *J. Chem. Soc., Dalton Trans.*, 1984, (7), 1349–1356, DOI: 10.1039/DT9840001349.

43 A. G. Blackman, E. B. Schenk, R. E. Jelley, E. H. Krenske and L. R. Gahan, Five-Coordinate Transition Metal Complexes and the Value of τ_5: Observations and Caveats, *Dalton Trans.*, 2020, **49**(42), 14798–14806, DOI: 10.1039/D0DT02985H.

44 N. Schweigert, R. W. Hunziker, B. I. Escher and R. I. L. Eggen, Acute Toxicity of (Chloro–)Catechols and (Chloro–)Catechol–copper Combinations in *Escherichia coli* Corresponds to Their Membrane Toxicity in Vitro, *Environ. Toxicol. Chem.*, 2001, **20**(2), 239–247, DOI: 10.1002/etc.5620200203.

45 M. J. Frisch, G. W. Trucks, H. B. Schlegel, G. E. Scuseria, M. A. Robb, J. R. Cheeseman, G. Scalmani, V. Barone, B. Mennucci, G. A. Petersson, H. Nakatsuji, M. Caricato, X. Li, H. P. Hratchian, A. F. Izmaylov, J. Bloino, G. Zheng, J. L. Sonnenberg, M. Hada, M. Ehara, K. Toyota, R. Fukuda, J. Hasegawa, M. Ishida, T. Nakajima, Y. Honda, O. Kitao, H. Nakai, T. Vreven, J. A. J. Montgomery, J. E. Peralta, F. Ogliaro, M. Bearpark, J. J. Heyd, E. Brothers, K. N. Kudin, V. N. Staroverov, R. Kobayashi, J. Normand, K. Raghavachari, A. Rendell, J. C. Burant, S. S. Iyengar, J. Tomasi, M. Cossi, N. Rega, J. M. Millam, M. Klene, J. E. Knox, J. B. Cross, V. Bakken, C. Adamo, J. Jaramillo, R. Gomperts, R. E. Stratmann, O. Yazyev, A. J. Austin, R. Cammi, C. Pomelli, J. W. Ochterski, R. L. Martin, K. Morokuma, V. G. Zakrzewski, G. A. Voth, P. Salvador, J. J. Dannenberg, S. Dapprich, A. D. Daniels, Ö. Farkas, J. B. Foresman, J. V. Ortiz, J. Cioslowski and D. J. Fox, *Gaussian 09, Revision D.01*, Gaussian, Inc., Wallingford, CT, 2009.

46 A. D. Becke, Density-Functional Exchange-Energy Approximation with Correct Asymptotic Behavior, *Phys. Rev. A*, 1988, **38**(6), 3098–3100, DOI: 10.1103/PhysRevA.38.3098.

47 J. P. Perdew, Density-Functional Approximation for the Correlation Energy of the Inhomogeneous Electron Gas, *Phys. Rev. B:Condens. Matter Mater. Phys.*, 1986, **33**(12), 8822–8824, DOI: 10.1103/PhysRevB.33.8822.

48 F. Weigend and R. Ahlrichs, Balanced Basis Sets of Split Valence, Triple Zeta Valence and Quadruple Zeta Valence Quality for H to Rn: Design and Assessment of Accuracy, *Phys. Chem. Chem. Phys.*, 2005, **7**(18), 3297–3305, DOI: 10.1039/B508541A.

49 A. V. Marenich, C. J. Cramer and D. G. Truhlar, Universal Solvation Model Based on Solute Electron Density and on a Continuum Model of the Solvent Defined by the Bulk Dielectric Constant and Atomic Surface Tensions, *J. Phys. Chem. B*, 2009, **113**(18), 6378–6396, DOI: 10.1021/jp810292n.

50 H. B. Schlegel, Geometry Optimization, *Wiley Interdiscip. Rev.:Comput. Mol. Sci.*, 2011, **1**(5), 790–809, DOI: 10.1002/wcms.34.

51 F. Neese, The ORCA Program System, *Wiley Interdiscip. Rev.: Comput. Mol. Sci.*, 2012, **2**, 73–78, DOI: 10.1002/wcms.81.

52 F. Neese, F. Wennmohs, U. Becker and C. Riplinger, The ORCA Quantum Chemistry Program Package, *J. Chem. Phys.*, 2020, **152**(22), 224108, DOI: 10.1063/5.0004608.

53 F. Neese, Software Update: The ORCA Program System—Version 5.0, *Wiley Interdiscip. Rev.: Comput. Mol. Sci.*, 2022, **12**(5), e1606, DOI: 10.1002/wcms.1606.

54 S. Grimme, S. Ehrlich and L. Goerigk, Effect of the Damping Function in Dispersion Corrected Density Functional Theory, *J. Comput. Chem.*, 2011, **32**, 1456–1465, DOI: 10.1002/jcc.21759.

55 S. H. Vosko, L. Wilk and M. Nusair, Accurate Spin-Dependent Electron Liquid Correlation Energies for Local Spin Density Calculations: A Critical Analysis, *Can. J. Phys.*, 1980, **58**(8), 1200–1211, DOI: 10.1139/p80-159.

56 C. Lee, W. Yang and R. G. Parr, Development of the Colle-Salvetti Correlation-Energy Formula into a Functional of the Electron Density, *Phys. Rev. B:Condens. Matter Mater. Phys.*, 1988, **37**(2), 785–789, DOI: 10.1103/PhysRevB.37.785.

57 A. D. Becke, Density–functional Thermochemistry. III. The Role of Exact Exchange, *J. Chem. Phys.*, 1993, **98**(7), 5648–5652, DOI: 10.1063/1.464913.

58 P. J. Stephens, F. J. Devlin, C. F. Chabalowski and M. J. Frisch, Ab Initio Calculation of Vibrational Absorption and Circular Dichroism Spectra Using Density Functional Force Fields, *J. Phys. Chem.*, 1994, **98**(45), 11623–11627, DOI: 10.1021/j100096a001.

59 F. Neese, An Improvement of the Resolution of the Identity Approximation for the Formation of the Coulomb Matrix, *J. Comput. Chem.*, 2003, **24**(14), 1740–1747, DOI: 10.1002/jcc.10318.

60 F. Neese, F. Wennmohs, A. Hansen and U. Becker, Efficient, Approximate and Parallel Hartree-Fock and Hybrid DFT Calculations. A "Chain-of-Spheres" Algorithm for the Hartree-Fock Exchange, *Chem. Phys.*, 2009, **356**(1–3), 98–109, DOI: 10.1016/j.chemphys.2008.10.036.

61 M. Garcia-Ratés and F. Neese, Effect of the Solute Cavity on the Solvation Energy and Its Derivatives within the Framework of the Gaussian Charge Scheme, *J. Comput. Chem.*, 2020, **41**(9), 922–939, DOI: 10.1002/jcc.26139.

62 B. Helmich-Paris, B. de Souza, F. Neese and R. Izsák, An Improved Chain of Spheres for Exchange Algorithm, *J. Chem. Phys.*, 2021, **155**(10), 104109, DOI: 10.1063/5.0058766.

63 F. Neese, The SHARK Integral Generation and Digestion System, *J. Comput. Chem.*, 2023, **44**(3), 381–396, DOI: 10.1002/jcc.26942.

64 R. D. Dennington II, T. A. Keith and J. M. Millam, *GaussView 6.0.16*, Semichem, Inc., Shawnee Mission, KS.

65 (*a*) A. M. B. Chandima, G. Sgro, S. M. Hilditch, U. I. Kaluarachchige Don, C. L. Ward, D. P. Anderson, L. Herman, D. Gelman, R. L. Lord and S. Groysman, CCDC 2456598: Experimental Crystal Structure Determination, 2025, DOI: 10.5517/ccdc.csd.cc2ng93k; (*b*) A. M. B. Chandima, G. Sgro, S. M. Hilditch, U. I. Kaluarachchige Don, C. L. Ward, D. P. Anderson,

L. Herman, D. Gelman, R. L. Lord and S. Groysman, CCDC 2456599: Experimental Crystal Structure Determination, 2025, DOI: 10.5517/ccdc.csd.cc2ng94l; (*c*) A. M. B. Chandima, G. Sgro, S. M. Hilditch, U. I. Kaluarachchige Don, C. L. Ward, D. P. Anderson, L. Herman, D. Gelman, R. L. Lord and S. Groysman, CCDC 2456600: Experimental Crystal Structure Determination, 2025, DOI: 10.5517/ccdc.csd.cc2ng95m.